Transition metal halide complexes of 4'-aminoacetophenone: Syntheses, structures, and magnetic behavior

Lyra Macek,[a] Julia C. Bellamy,[a] Kesli Faber,[a] Conor R. Milson,[a] Christopher P. Landee,[b] Diane A. Dickie,[c] and Mark M. Turnbull.[a*]

[a]Carlson School of Chemistry and Biochemistry, Clark University, 950 Main St., Worcester, MA 01601, USA

[b]Dept. of Physics, Clark University, 950 Main St., Worcester, MA 01601, USA

[c]Dept of Chemistry, University of Virginia, 409 McCormick Road, Charlottesville, VA 22904, USA

Abstract:

A family of eight compounds of the general formula $[(C_8H_9NO)_2MX_2]$ or $[(C_8H_9NO)_2(H_2O)_2MX2]$, (M=Ni, Co, Cu, Zn; X=Cl, Br) has been prepared and the compounds characterized by combustion analysis, IR, single-crystal X-ray diffraction and variable temperature magnetization measurements. $[[(C_8H_9NO)_2(H_2O)_nMX2]$, (**1**, n=0, M=Cu, X=Cl; **2**, n=0, M=Cu, X=Br; **3**, n=2, M=Ni, X=Cl; **4**, n=2, M=Ni, X=Br; **5**, n=2, M=Co, X=Cl; **6**, n=2, M=Co, X=Br; **7**, n=0, M=Zn, X=Cl; **8**, n=0, M=Zn, X=Br.) The eight compounds crystallize in three distinct space groups and have coordination number of either four (compounds **1**, **2**, **7**, and **8**) or six (compounds **3**-**6**). Compounds **1** and **2** are slightly distorted square planar, compounds **3**-**6** are slightly distorted octahedral, and compounds **7** and **8** are slightly distorted tetrahedral. All eight compounds form chains either through bihalide interactions (**1** and **2**) or systems of hydrogen bonds (**3**-**8**). Chains are linked into layers through short halide…halide (**1**, **2**, **7**) and both traditional and non-traditional hydrogen bonds. The complexes have also been studied via variable temperature magnetic susceptibility measurements. Data for Cu(II) complexes **1** and **2** the 1D-Heisenberg uniform chain model with J/k_B of -13.4(6) K and -14.3(4) K, respectively, with antiferromagnetic interchain interactions (θ = -4.1(5) K, -2.5(5) K, respectively) following the $H = -J\sum s_i \cdot s_j$ Hamiltonian. The Ni(II) and Co(II) compounds showed temperature dependent moments which were well-modeled as arising due to single-ion anisotropy.

1. Introduction

The discovery of the correlation between magnetism and electricity in the 19th century brought about a newfound interest in magnetic research. Broader interest in magnetism occurred after the discovery of single-molecule magnets (SMM) [1,2,3], single-chain magnets (SCM) [4,5,6] and single-ion magnets (SIM) [7,8,9] magnets. Investigation into these families of compounds continues in SMM [10,11], SCM [12,13,14] and SIM [15,16,17,18], respectively. These discoveries demonstrated the importance of studying magnetism in the context of coordination chemistry [19,20,21,22], with the intent of gaining a better understanding of magneto-structural relationships. Considerable work has gone into exploring variables that could potentially affect the magnetic exchange within a structure, in particular in lanthanide [23,24,25], polyoxometalate [26,27,28,29], metal organic frameworks [30,31,32], and transition metal complexes [33,34,35,36]. The sheer quantity of recent publications demonstrates the degree of interest in utilizing transition metal complexes to study molecular magnetic materials. Transition metal complexes have been used as a method of research in areas such as the magnetocaloric effect [37,38,39], spin-exchange [40,41], and ferromagnetism and ferroelectricity [42]. An intriguing area of study for such complexes originates from the complexes' lattice properties and the presence of interactions between non-bonded atoms. A significant hole in our collective knowledge of magnetism revolves around the lack of our ability to control such interactions as a means to control the magnetic superexchange. Organic components in these transition metal complexes provide a variable that can be manipulated and controlled. A very slight change in the steric properties of the organic moiety can greatly affect the magnetic properties of the entire crystal [43]. Hopefully, by comparing the effects of small changes within the organic component, these molecular magnetic materials will be more easily customizable.

A specific area of research in molecular magnetism that is of current interest has focused on transition metal halide complexes with various nitrogen-donor ligands, such as substituted pyridines [44,45,46,47,]. There has been particular interest in using heterocyclic, nitrogen-donating ligands in these complexes, such as substituted pyridines, quinoline [48,49], and isoquinoline [50,51,52]. Aromatic amines, such as aniline, have also been proven as effective ligands for the preparation of complexes of this type. Aniline and substituted aniline compounds have been studied for their qualities as Lewis bases and for how their basicity affects reactions

and reaction mechanisms in the synthesis of complexes with the formula ML_2X_2 (X = Cl, Br; L = aniline-based ligand). [53, 54, 55,56,57]

In aniline, because the nitrogen is the only substituent on the six-membered ring and is sp^2 hybridized, the molecule is almost completely flat. Adding substituents that have different properties which reduce the planarity of the molecule can affect the way in which these molecules interact and pack together. Work has been done to examine the effect when the 4-position of aniline is substituted with a strong electron donor (hydroxy) [58,59], weak electron donor (methyl), [60,61] and weak electron-withdrawing groups (halogens) [60]. We have previously studied the magneto-structural correlation of chloro-, methyl, and methoxy substituents in the para position of aniline [60, 62, 63]. However, we find little information published on the effect of a strongly withdrawing substituent. In order to begin to understand the effects of an electron-withdrawing substituent on the overall magneto-structural relationships of a complex, we prepared a family of compounds that used 4'-aminoacetophenone (4'-AAP) as the ligand which incorporates an electron-withdrawing ketone functionality. The ketone is strongly polar, it can act as a hydrogen bond acceptor, and the oxygen atom has the potential to compete with the nitrogen atom and coordinate with the metal. These characteristics enable different interactions and crystal packing, making it a very valuable area of study.

Here we report the synthesis, characterization, single crystal X-ray structures, and magnetic analysis of eight complexes in the family of compounds with the general formula $[(C_8H_9NO)_2(H_2O)_nMX2]$ (**1**, n=0, M=Cu, X=Cl; **2**, n=0, M=Cu, X=Br; **3**, n=2, M=Ni, X=Cl; **4**, n=2, M=Ni, X=Br; **5**, n=2, M=Co, X=Cl; **6**, n=2, M=Co, X=Br; **7**, n=0, M=Zn, X=Cl; **8**, n=0, M=Zn, X=Br.). Our intention behind this work was to create a family of compounds that would expand the library of knowledge the scientific community has created in order to better understand how 3D structure affects magnetic properties. This family in particular sheds light on the effects a strong electron withdrawing substituent in the para position of aniline has on the structural and magnetic properties of a family of transition metal halide complexes. We hope by producing sufficient families of such compounds, we can gain the ability to create magnets with more specific and customizable properties.

2. Experimental

Copper (II) chloride dihydrate and nickel (II) chloride hexahydrate were purchased from J.T. Baker. Cobalt (II) bromide, cobalt (II) chloride hexahydrate and zinc (II) chloride tetrahydrate were purchased from Aldrich Chemical Company. Zinc (II) bromide was purchased from AlfaAesar; nickel (II) bromide was purchased from Thiokol; copper (II) bromide was purchased from Fischer Scientific. 1-Propanol was purchased from OmniSolvents. 4'-Aminoacetophenone [4'-AAP] was purchased from Acros Organics. All materials were used as received. The IR data were collected by ATR on a Perkin-Elmer Spectrum 100. X-Ray powder diffraction data were collected using a Bruker AXS-D8 Focus X-ray Powder Diffractometer. Elemental Analyses were carried out by the Marine Science Institute, University of California, Santa Barbara CA 93106. No efforts were made to maximize yields.

2.1. Bis(4'-aminoacetophenone)dichloridocopper(II), [(4'-AAP)$_2$CuCl$_2$] (**1**)

$CuCl_2 \cdot 2H_2O$ (0.170g, 1.00 mmol) was dissolved in 10ml of 1-propanol producing a bright green solution. 4'-AAP (0.272g, 2.01 mmol) was dissolved in 10ml of 1- propanol resulting in a colorless solution. The solution of $CuCl_2 \cdot 2\ H_2O$ was added to the solution of 4'-AAP. The combined solution was deep brown and a precipitate appeared immediately as the two solutions were combined. The precipitate contained single crystals and was isolated using vacuum filtration and washed with ~ 2ml of 1- propanol and air-dried to give a light brown powder, 0.359g (88.7%). IR (ν in cm-1): 3301 m, 3217 m, 3117 w, 1682 s, 1604 s, 1568 m, 1507 w, 1428 m, 1360 m, 1304 m, 1268 s, 1226 m 1175 m, 1106 w, 1076 s, 1023 m, 961 m, 831 s, 727 w, 689 m, 591 m. CHN for $C_{16}H_{18}N_2O_2Cl_2Cu$, found (calc.): C, 47.59 (47.48): H, 4.40 (4.48): N, 6.90 (6.92).

2.2. Bis(4'-aminoacetophenone)dibromidocopper(II), [(4'-AAP)$_2$CuBr$_2$] (**2**)

$CuBr_2$ (0.223g, 1.00 mmol) and 4'- aminoacetophenone (0.271g, 2.01mmol) were dissolved separately, each in 5ml of 1- propanol. The solution of $CuBr_2$ was dark brown with hints of green. The solution of 4'-AAP was added to the solution of $CuBr_2$. The combined solution appeared dark brown and had tints of amber yellow. No precipitate formed immediately, so the solution was moved to a desiccator and left for 24 hours. A precipitate had formed along the bottom, which was isolated using vacuum filtration and air dried. The precipitate was put in 5ml of acetone to dissolve an impurity. The mixture of acetone and solid was filtered using

vacuum filtration to isolate the remaining precipitate that contained single crystals and left to dry, 78mg were collected total (15.8%). IR (ν in cm-1): 3284 m, 3210 m, 3109 w, 1684 s, 1603 s, 1564 m, 1506 w, 1426 w, 1359 s, 1304 w, 1267 s, 1223 m, 1177 w, 1086 s, 1016 w, 961 m, 831 s, 725 w, 682 s. 631 w, 591 m. CHN for $C_{16}H_{18}N_2O_2Br_2Cu$, found (calc.): C, 35.99 (36.83); H, 3.32 (3.66); N, 5.18 (5.57).

2.3. Bis-(4'-aminoacetophenone)diaquadichloridonickel(II), [(4'-AAP)$_2$(H$_2$O)$_2$NiCl$_2$] (**3**)

$NiCl_2 \cdot 6\ H_2O$ (0.238g, 1.00 mmol) was heated gently in 10ml of 1-propanol until the solid was completely dissolved. 4'- AAP (0.270g, 2.00 mmol) was dissolved in 10ml of 1-propanol. The solution of $NiCl_2 \cdot 6\ H_2O$ was added to the solution of 4'-AAP. Once combined, the solution was a translucent bright fluorescent green color. No precipitate appeared immediately so it was left to evaporate slowly. After 24 hours, a bright green powder had formed along the bottom, which was isolated with vacuum filtration and washed with 2ml of 1-propanol, 0.196g (44.9%). After 30 days, crystals formed along the edge of the beaker containing the filtrate that had been left to crystallize further, which were collected and used for the single-crystal X-ray diffraction. IR (ν in cm-1): 3345 m, 3318 m, 3232 m, 3152 m, 1662 s, 1602 s, 1559 w, 1514 w, 1433 m, 1362 m, 1306 w, 1281 s, 1306 s, 1179 w, 1019 s, 1003 s, 951 m, 834 s, 697 w, 621 m, 592 m. CHN for $C_{16}H_{22}N_2O_4Cl_2Ni$, found (calc.): C, 43.86 (44.08); H, 5.08 (5.09); N, 6.285 (6.426).

2.4. Bis-(4'-aminoacetophenone)diaquadibromidonickel(II), [(4'-AAP)$_2$(H$_2$O)$_2$NiBr$_2$] (**4**)

$NiBr_2$ (0.216g, 0.988 mmol) and 4'-AAP (0.269g, 1.99 mmol) were dissolved separately, each in 5ml of 1- propanol. The solution of $NiBr_2$ was added to the solution of 4'-AAP in a 25ml beaker. No precipitate appeared immediately so the solution was left to evaporate slowly. After four days, a precipitate containing single crystals had formed along the bottom which was isolated by vacuum filtration and washed with ~10 drops of 1- propanol. The precipitate was air dried, 0.206g (39.2%). IR (ν in cm-1): 3369 m, 3302 m, 3225 m, 3147 m, 1663 s, 1602 s, 1558 m, 1432 m, 1359 m, 1278 s, 1254 s, 1178 w, 1107 w, 1030 s, 962 m, 834 s, 695 w, 589 m. CHN for $C_{16}H_{22}N_2O_4Br_2Ni$, found (calc.): C, 36.46 (36.61); H, 4.3 (4.2); N, 5.315 (5.337).

2.5. Bis-(4'-aminoacetophenone)diaquadichloridocobalt(II), [(4'-AAP)$_2$(H$_2$O)$_2$CoCl$_2$] (**5**)

$CoCl_2 \cdot 6\ H_2O$ (0.239g, 1.00 mmol) was dissolved in 12ml of 1-propanol, producing a royal blue solution. 4'- aminoacetophenone (0.270g, 2.00 mmol) was dissolved in 10ml of 1-propanol. The solution of 4'- aminoacetophenone was added to the solution of $CoCl_2 \cdot 6\ H_2O$. The

combined solution maintained the royal blue color, and no precipitate appeared immediately. The solution was left for a week to evaporate slowly in the air. In that time a bright pink precipitate had formed, the solution was filtered using vacuum filtration and washed with 3ml of 1-propanol. The precipitate was air dried and contained single crystals, 0.090g (20.6%). IR (ν in cm-1): 3324 m, 3235 m, 3157 w, 1661 s, 1602 s, 1513 w, 1434 m, 1362 m, 1306 w, 1282 s, 1260 s, 1179 m, 1162 w, 1107 m, 1014 m, 985 s, 950 m, 833 s, 695 m, 647 m, 594 s. CHN for $C_{16}H_{22}N_2O_4Cl_2Co$ (calc.): C, 44.53 (44.16): H, 5.083 (4.885); N, 6.445 (6.422).

2.6. Bis-(4'-aminoacetophenone)diaquadibromidocobalt(II), [(4'-AAP)$_2$(H$_2$O)$_2$CoBr$_2$] (**6**)

$CoBr_2$ (0.217g, 0.992 mmol) and 4'-AAP (0.269g, 1.99 mmol) were dissolved separately, each in 5ml of 1- propanol. The solution of $CoBr_2$ was added to the solution of 4'-AAP and once combined, appeared as a dark royal blue solution. No precipitate appeared immediately so the beaker was put in a desiccator and allowed to evaporate. After four days a pink precipitate had formed along the bottom, which was isolated using vacuum filtration and airdried, 0.111g (21.1%). IR (ν in cm-1): 3344 m, 3306 m, 3228 m, 3146 m, 1661 s, 1600 s, 1511 w, 1431 m, 1359 m, 1305 w, 1278 s, 1255 s, 1178 m, 1107 w, 1016 s, 999 s, 961 m, 833 s, 694 m, 590 m. CHN for $C_{16}H_{22}N_2O_4Br_2Co$, found (calc.): C, 36.60 (36.60); H, 4.175 (4.223); N, 5.09 (5.34).

2.7. Bis (4'-aminoacetophenone)dichloridozinc(II), [(4'-AAP)$_2$ZnCl$_2$] (**7**)

$ZnCl_2 \cdot 4\ H_2O$ (0.211g, 1.01mmol) and 4'-AAP (0.271g, 2.01mmol) were dissolved separately, each in 5ml of 1-propanol. The solution of $ZnCl_2 \cdot 4\ H_2O$ was slowly added to the solution of 4'-AAP resulting in a very faint pale-yellow solution. This was left to evaporate slowly. After 11 days of evaporation, the remaining solution was put into a desiccator. Five days later, crystals that had formed along the sides were pushed into the solution. The following day the precipitate was isolated using vacuum filtration, washed with ~3 drops of 1-propanol, and air dried, 0.030g (7.37%). IR (ν in cm-1): 3404 m + b, 3265 m, 3224 m, 3135 w, 1675 s, 1605 s, 1509 w, 1430 w, 1360 m, 1305 w, 1267 s, 1220 m, 1177 m, 1076 s, 1023 m, 963 m, 838 s, 724 m, 680 s, 593 m.

2.8. Bis (4'-aminoacetophenone)dibromidozinc(II), [(4'-AAP)$_2$ZnBr$_2$] (**8**)

$ZnBr_2$ (0.225g, 1.00 mmol) and 4'-AAP (0.271g, 2.01mmol) were dissolved separately, each in 5ml of 1- propanol. The solution of $ZnBr_2$ was added to the solution of 4'-AAP, resulting in a colorless solution, which allowed to evaporate slowly. After two weeks, the solution was moved to a desiccator. A week later, the solution was removed from the desiccator and was

returned to the desktop. The following day crystals had formed along the top edge of the beaker and parafilm. Some were collected for analysis while the rest were pushed back into the solution. The crystals were collected using a plastic scapula and washed with ~5 drops of 1- propanol, 0.023g (4.65%). IR (ν in cm-1): 3257 w, 3212 w, 3112 w, 1685 m, 1670 m, 1604 s, 1508 w, 1431 w, 1360 m, 1306 w, 1270 s, 1226 w, 1181 w, 1119 w, 1064 s, 958 m, 839. CHN for $C_{16}H_{22}N_2O_4Br_2Zn$, found (calc.): C, 38.87 (38.78); H, 3.63 (3.66); N, 5.69 (5.65).

2.9. Magnetic Data

Magnetic data for compounds **1**-**6** were measured on a Quantum Design MPMS-XL magnetometer (SQUID). Crystals were powdered prior to measurements and powder X-ray diffraction used to confirm the phase of the material (by comparison with single crystal data) and purity (no unindexed peaks were detected). Samples were placed in a gelatin capsule which was then affixed inside a plastic straw. Magnetization was measured in applied fields ranging from 0 to 10 kOe. As the field was reduced back to zero, several data points were recollected to check for hysteresis; none was observed. However, the Ni and Co samples (compounds **3-6**) showed small deviations as the field returned to zero due to the intrinsic anisotropy of the ions and sample reorientation. M(H) was linear to at least 5 kOe for all samples measured. Magnetization was then measured between 1.8 and 310 K in an applied field of 1 kOe. All data were corrected for the background of the gelatin capsule and straw (measured independently) as well as the diamagnetic contributions of the constituent atoms, estimated via Pascal's constants [64]. Data were fit using the $H = -J \sum s_i \cdot s_j$ Hamiltonian.

2.10. Single- crystal X-ray diffraction data

X-ray diffraction data for structures **1**–**8** were collected on a Bruker Kappa DUO diffractometer. Data collection, reduction and absorption corrections were made using Bruker Instrument Services v.2012.12.0.3, SAINT v.8.34A and SADABS v.2014/5 [65]. The structures were solved using SHELXS-2014[66] and refined via least squares analysis with SHELXL-2018/3[67]. Non-hydrogen atoms were refined using anisotropic thermal parameters. Hydrogen atoms bonded to carbon atoms were placed in calculated positions and refined using a riding model and isotropic thermal parameters. Hydrogen atoms bonded to nitrogen or oxygen were located in the difference Fourier maps and their positions refined with fixed isotropic thermal parameters. One ligand in the structure of compound **8** is two-site disordered with refined occupancies of 0.827(6) and 0.173(6). Equivalent atoms in the two components were restrained

to have similar U_{ij} values. Crystallographic information for compounds **1**–**8** is given in Table 1. Selected bond lengths and angles are presented in Table 2 while hydrogen bonding parameters are shown in Table 3. The data have been deposited with the CCDC: **1**, 2211686; **2**, 2211687; **3**, 2211688; **4**, 2211689; **5**, 2211690; **6**, 2211691; **7**, 2211692; **8**, 2211693.

Table 1

Crystal and experimental data for **1-8.**

	1	**2**	**3**	**4**	**5**	**6**	**7**	**8**
Formula	$C_{16}H_{18}N_2O_2Cl_2Cu$	$C_{16}H_{18}N_2O_2Br_2Cu$	$C_{16}H_{22}N_2O_4Cl_2Ni$	$C_{16}H_{22}N_2O_4Br_2Ni$	$C_{16}H_{22}N_2O_4Cl_2Co$	$C_{16}H_{22}N_2O_4Br_2Co$	$C_{16}H_{18}N_2O_2Cl_2Zn$	$C_{16}H_{18}N_2O_2Br_2Zn$
MW (g/mol)	404.76	493.68	435.96	524.88	436.18	525.10	406.59	495.51
T (K)	100(2)	100(2)	100(2)	100(2)	100 (2)	100(2)	100(2)	100(2)
λ (Å)	1.54178	0.71073	0.71073	0.71073	0.71073	0.71073	0.71073	0.71073
Crystal system	triclinic	triclinic	triclinic	triclinic	triclinic	triclinic	monoclinic	monoclinic
Space group	*P*-1	*P*-1	*P*-1	*P*-1	*P*-1	*P*-1	*I*2/a	$P2_1/c$
a (Å)	4.4885(3)	4.5231(4)	5.5973(5)	5.7222(2)	5.6178(2)	5.7429(2)	11.4937(5)	4.8661(3)
b (Å)	5.9498(4)	6.1949(5)	8.5535(7)	8.3851(3)	8.6334(3)	8.4420(3)	4.6318(2)	20.6633(16)
c (Å)	15.3913(12)	15.2430(15)	9.6923(8)	9.9223(4)	9.6883(3)	9.9260(4)	31.7180(14)	17.7139(12)
α(°)	93.876(2)	95.420(3)	79.516(3)	79.3906(14)	79.4467(10)	79.4112(12)	90	90
β (°)	90.422(2)	91.051(3)	85.217(3)	86.4999(13)	84.9876(9)	86.3938(13)	96.3880(14)	94.570(3)
γ(°)	92.694(2)	94.288(3)	80.008(3)	82.2297(13)	79.4838(8)	82.1697(12)	90	90
V (Å^3)	409.62(5)	423.87(7)	448.72(7)	463.33(3)	453.47(3)	468.27(3)	1678.07(13)	1775.5(2)
Z	1	1	1	1	1	1	4	4
Size (mm)	0.123 x 0.058 x 0.040	0.127 x 0.088 x 0.033	0.196 x 0.130 x 0.050	0.104 x 0.054 x 0.044	0.406 x 0.067 x 0.047	0.099 x 0.048 x 0.043	0.234 x 0.044 x 0.021	0.092 x 0.021 x 0.015
Abs. coef. (mm^{-1})	4.969	6.011	1.402	5.382	1.264	5.206	1.791	5.894
F(0,0,0)	207	243	226	262	225	261	832	976
Range (°)	2.878- 68.210	2.685-28.319	2.140-29.574	2.09-28.282	2.435-33.139	2.089-28.321	2.585-27.473	1.971--28.310
Index ranges	$-5\leq h\leq 5$ $-7\leq k\leq 7$ $0\leq l\leq 18$	$-6\leq h\leq 6$ $-8\leq k\leq 8$ $0\leq l\leq 20$	$-7\leq h\leq 7$ $-11\leq k\leq 11$ $-13\leq l\leq 13$	$-7\leq h\leq 7$ $-11\leq k\leq 11$ $-13\leq l\leq 12$	$-8\leq h\leq 6$ $-13\leq k\leq 13$ $-14\leq l\leq 14$	$-7\leq h\leq 7$ $-10\leq k\leq 11$ $-13\leq l\leq 13$	$-14\leq h\leq 14$ $-5\leq k\leq 5$ $-41\leq l\leq 41$	$-6\leq h\leq 6$ $-27\leq k\leq 23$ $-23\leq l\leq 23$
Rfln. Coll.	1473	2094	2501	2298	3453	2332	1907	4421
Ind. Rfln (R_{int})	1453	2032	2412	2148	3107	2183	1754	3703
Data/restraints/ para.	1473/1/113	2094/0/113	2501/0/128	2298/0/128	3453/1/128	2332/2/128	1907/0/112	4421/72/293
Final R (R_1) [I>2σ(I)] (wR_2)	0.0466 0.1338	0.0281 0.0649	0.0180 0.0460	0.0192 0.0386	0.0214 0.0547	0.0210 0.0405	0.0228 0.0525	0.0366 0.0622

R index R_1 (all data) (wR_2)	0.0468 0.1340	0.0295 0.0655	0.0188 0.0188	0.0221 0.0393	0.0255 0.0566	0.0237 0.0237	0.0264 0.0538	0.0493 0.0649
Final peak/ hole (e/ Å^3)	0.736/ -0.490	0.681/ -0.765	0.452/ -0.328	0.402/ -0.444	0.540/ -0.330	0.524/ -0.688	0.372/ -0.219	0.541/ -0.560

3. Results

3.1. Synthesis

The reaction of 4'-aminoacetophenone with the various metal halides (M= Cu, Ni, Co, Zn; X= Cl, Br) yielded complexes **1**-**8** in yields ranging from 4.5 to 88% (Scheme 1). Although the desired products were the ML_2X_2 compounds, both ML_2X_2 and $ML_2(H_2O)_2X_2$ compounds were obtained after crystallization. The reaction is very tolerant to the choice of the reaction solvent: solution syntheses utilizing a variety of solvents and solvent mixtures (methanol, ethanol, acetone, 1-propanol) were effective. 1-Propanol was more efficient/ effective in producing high quality single crystals. No significant difference in yield was observed between different alcohols. Attempts were made to crystallize the anhydrous versions of compounds **3**-**6**, via changes to solvent properties as well as reaction conditions, but were unsuccessful.

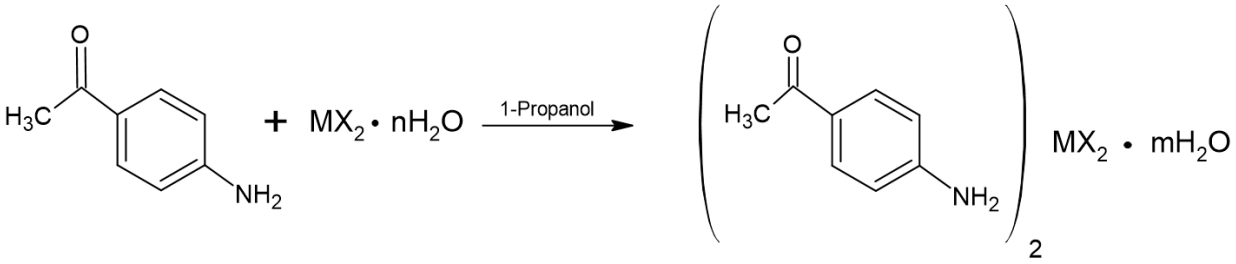

Scheme 1- Synthesis of compounds **1**-**8**. (M=Cu, Ni, Co, Zn; X=Cl, Br; n=0, 2, 4, 6; m=0, 2)

3.2. Crystal Structures

Compounds **1** and **2** crystallize in the triclinic space group *P*-1 with one halide ion, one 4'-aminoacteophenone ligand and one-half Cu(II) ion comprising the asymmetric unit [68]. The Cu(II) ion is positioned on a crystallographic inversion center and as such, its coordination sphere contains two halide ions and two 4'-AAP molecules in a square-planar geometry (see Figure 1). Selected bond lengths and angles are provided in Table 2. The Cu-N bonds in compounds **1** and **2** are 2.026(4)Å and 2.019(3)Å, respectively, and are comparable to those seen in other di-aniline complexes with coordinated anions such as $[(C_7H_7NO_2)_2CuCl_2]$ [69] and $[(C_6H_7N_2)_2CuCl_2]$ [70].The Cu-Cl bond is 2.263(9)Å and the Cu-Br bond is 2.422(4) Å; these values agree with those of compounds with similar bonds such as trans-$[Cu(py)_2X_2]$ [71,72]. All *trans* bond angles are 180° as required by symmetry. The aromatic ring is virtually planar (mean

deviation of constituent atoms= 0.0059Å) in **1**, with both the carbon atom of the carbonyl substituent (0.0602Å) and N11 atom (0.0432Å) nearly in the same plane. Due to conjugation with the ring the carbonyl group in each of these compounds is nearly coplanar with the aromatic ring, the O17-C17-C14-C15 torsion angles in compounds **1** and **2** are 0.6° and 0.8°, respectively. The aniline N-atom becomes nearly tetrahedral after coordination; the Cu-N11-C11 and Cu-N11-H1A angles average 109.5° compared to the free ligand where the N- atom is sp^2 hybridized due to conjugation (∠H11A-N11-C1=116°). The greatest distortion from tetrahedral geometry occurs with the Cu-N11-C11 angle, 118(3)°, most likely due to steric pressure. The planes of the aromatic rings are inclined ~61.5° to opposite faces from the Cu(II) coordination plane, which likely occurs to promote π-stacking of aromatic rings.

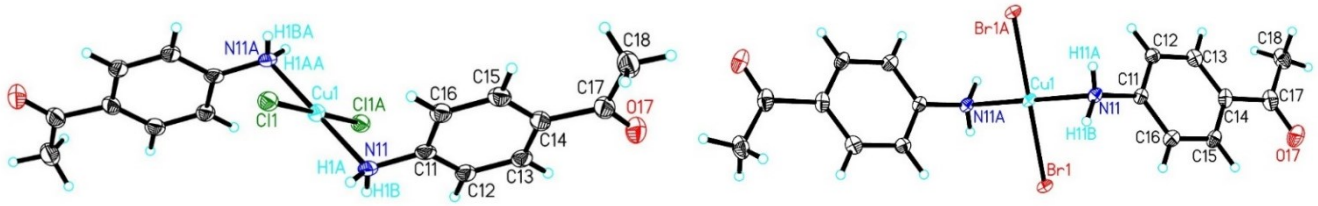

Figure 1:A thermal ellipsoid plot (50%) of the molecular unit of **1** (left) and **2** (right). Only the asymmetric unit, Cu-coordination sphere, and those hydrogen atoms whose positions were refined are labeled.

Table 2
Selected bond lengths (Å) and angles **(**°) for **1**-**8**

	1	**2**	**3**	**4**	**5**	**6**	**7**	**8**
Bond Lengths								
M1-X1	2.2629(9)	2.4219(4)	2.4217(3)	2.57109(18)	2.4514(2)	2.60765(19)	2.2465(4)	2.3617(5)
M1-N11	2.026 (4)	2.019(3)	2.1191(9)	2.1198(15)	2.1834(8)	2.1824(16)	2.0542(14)	2.068(3)
N11-C11	1.433(5)	1.441(5)	1.4238(12)	1.422(2)	1.4171(11)	1.422(2)	1.443(2)	1.439(4)
M1-O1W			2.0552(8)	2.0583(13)	2.0682(7)	2.0659(13)		
Bond Angles								
N11-M1-X1	88.84(11)	91.03(9)	87.19(3)	92.77(4)	92.86(2)	92.71(4)	108.95(4)	105.84(9)
C11-N11-M1	118.0(3)	118.9(2)	121.97(6)	122.14(11)	121.95(6)	122.06(12)	111.10(10)	109.9(2)
O1W-M1-N11			94.36(3)	93.04(6)	84.99(3)	93.57(6)		
O1W-M1-X1			89.37(3)	89.82(4)	89.70(2)	89.84(4)		

Table 3 Hydrogen bonding for compounds **1-8**

Compound	D-H···A	d(D-H) Å	d(H···A) Å	d(D··· *A*) Å	<(DHA)°
1					
	N11-H11B··· *X1A*	0.84(2)	2.62(3)	3.417(4)	159(5)
2					
	N11-H11A···X1B	0.84(5)	2.70(5)	3.125(3)	113(4)
	N11-H11B···X1C	0.96(5)	2.71(4)	3.571(3)	150(3)
3					
	OW1-H1A···X1D	0.804(17)	2.311(17)	3.1038(9)	169.1(15)
	OW1-H1B··· O17E	0.767(17)	1.969(17)	2.7172(11)	165.1(16)
	N11-H11A··· X1*D*	0.879(15)	2.520(15)	3.3675(9)	162.1(12)
4					
	OW1-H1A···X1F	0.77(2)	2.50(2)	3.2505(14)	166(2)
	OW1-H1B··· O17G	0.81(2)	1.94(2)	2.7298(19)	164(2)
	N11-H11B··· X1*F*	0.87(2)	2.66(2)	3.4570(15)	153.8(18)
5					
	OW1-H1B···X1H	0.783(13)	2.334(13)	3.0978(8)	165.6(15)
	OW1-H1A··· O17E	0.801(16)	1.921(16)	2.7062(10)	166.3(15)
	N11-H11B··· X1*H*	0.873(15)	2.515(15)	3.3545(9)	161.6(13)
6					
	OW1-H1A···X1I	0.805(16)	2.457(17)	3.2431(14)	166(2)
	OW1-H1B··· O17G	0.806(16)	1.931(17)	2.7179(18)	165(2)
	N11-H11B··· X1*I*	0.83(2)	2.67(2)	3.4463(16)	158(2)
7					
	N11-H11A··· X1J	0.85(2)	2.93(2)	3.4230(14)	118.7(15)
	N11-H11A··· X1K	0.85(2)	2.65(2)	3.4750(15)	162.9(17)
	N11-H11B··· X1L	0.88(2)	2.59(2)	3.3610(15)	147.4(16)
8					
	N21-H21A··· X1M	0.92(4)	3.00(4)	3.563(3)	121(3)
	N21-H21A··· X1N	0.92(4)	2.84(4)	3.669(3)	151(3)
	N21-H11B··· X2M	0.85(4)	2.66(4)	3.432(3)	152(3)
	N11-H11B··· *O27O*	0.87(4)	2.17(4)	2.963(4)	156(4)

Symm. Op.: A (x, y+1, z), B (-x+2, -y, -z), C (-x+2, -y+1, -z), D (x-1, y, z), E (x, y+1, z-1), F (-x+1, -y+1, -z+1), G (x, y-1, z+1), H (-x, -y+1, -z+1), I (-x+1, -y, -z), J (x, y-1, z), K (-x+2, -y, -z+1), L (-x+3/2, y-1, -z+1), M (x+1, y, z), N (-x, -y+1, -z), O (x+1, -y+3/2, z+1/2)

The unit-cell translation related molecules are linked into chains parallel to the *a*- axis via semi-coordinate bonds between the Cu ion and the halide ions of adjacent $(4'\text{-AAP})_2CuX_2$ units along the *a*-axis [symm. transform A = *x-1, y, z*] (Figure 2a). In compound **1**, the Cu1…Cl1a distance is 3.415(9) Å and the Cu1-Cl1…Cu1a angle is 102.57(6)°, both of which are comparable to values of similar compounds reported to have bihalide interactions such as $[(C_4H_5N_3)CuCl_2]$ and $[(C_4H_5N_3)_2CuCl_2]$ [73]. The chains are linked parallel to the *b*-axis via short chloride…chloride contacts to form layers parallel to the *ab*-plane; the Cl1-Cl1a distance is 3.656(4) Å and Cu1-Cl1-Cl1a angle is 137.03(11)°. Although the distance between chloride ions is slightly larger than the sum of the ionic radii, the Cu1-Cl1…Cl1A-Cu1A torsion angle is 180° and meets the criteria for two-halide magnetic exchange interactions [74]. Nontraditional hydrogen bonds between the C18 methyl substituents of one molecular unit and the O17 carbonyl oxygen atom of an adjacent unit ($d_{(D\ldots A)}$ = 3.488(14) Å) link the layers together parallel to the *c*-axis (Figure 2b). These interactions help stabilize the crystal lattice by supporting an organized and uniform stacking of the aromatic rings with an interplanar separation of 3.301 Å. The location of the non-traditional hydrogen bonds suggests the primary 2D crystal structure is dictated by the bihalide and two-halide interactions, and the non-traditional hydrogen bonds maintain the 3D form.

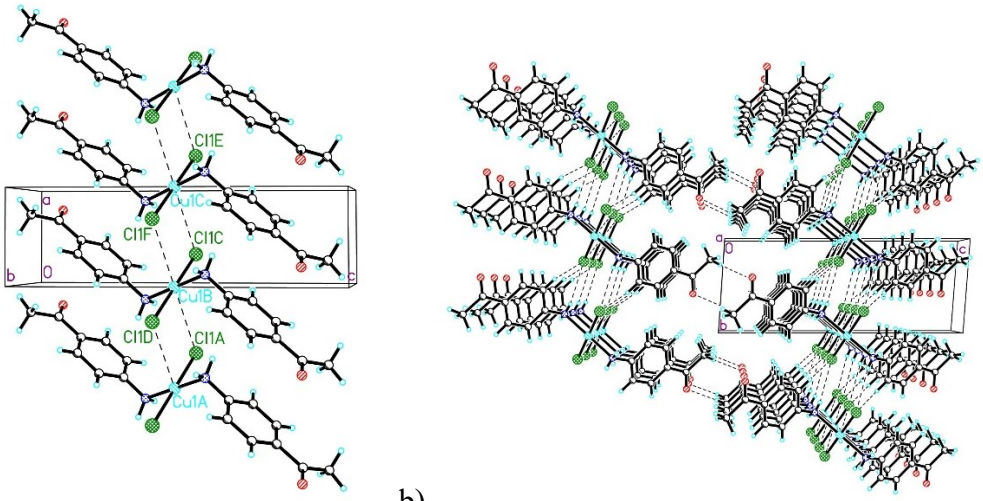

a) b)

Figure 1: The structure of compound **1** showing bihalide chain formation (a) and packing of the chains highlighting nontraditional hydrogen bonds (b).

There are no significant differences in the crystal packing of compounds **1** and **2**. The slight differences present are a result of the different halide ions and are comparable with the increase

in ionic radius of the bromide ion. Figures of the asymmetric units of **1** and **2**, as well as packing diagrams of compound **2** showing the chain and layer formation, and hydrogen bonding, are included in the SI (Figures S1-S5).

The $L_2(H_2O)_2\,MX_2$ complexes (**3-6)** crystallize as distorted octahedra and share the same crystal class, space group, and general packing structure; only compound **3** is discussed in detail. Compound **3** crystallizes in the triclinic space group *P*-1 with one chloride ion, one 4'-AAP ligand, one water molecule, and one-half Ni(II) ion comprising the asymmetric unit (see Figure 3a) (Figures showing the asymmetric units may be found in the SI as Figures S6, S7, S10 and S13 for **3-6** respectively). Similar to compounds **1** and **2**, the Ni(II) ion is located on an inversion center; as such, the coordination sphere comprises two 4'-AAP ligands, two chloride ions, and two coordinated water molecules. The Ni-Cl bond lengths (Table 2) agree with those previously reported for compounds with similar coordination spheres such as $[Ni(4\text{-}Clan)_2Cl_2(MeOH)_2]$ [63]. The aromatic ring is virtually planar (mean deviation of constituent atoms = 0.0043Å), with both the C17 atom (0.0244Å) and N11 atom (0.0226Å) are nearly in the same plane. Similar to compounds **1** and **2**, conjugation causes the carbonyl to be nearly coplanar with the ring; the O17-C17-C14-C15 torsion angle is 2.2°. This value is slightly greater than in compounds **1** and **2**, but remains a very small. The N11-Ni1-Cl1 and O1W-Ni1-N11 angles average 90°, indicating a very slight distortion from octahedral geometry. The planes of the aromatic rings in each molecular unit are inclined 60.68° from the Cl1-Ni-N11 plane in opposite directions.

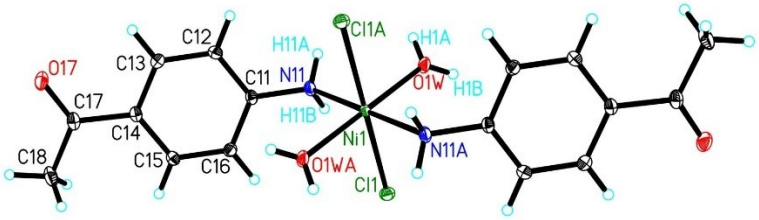

a)

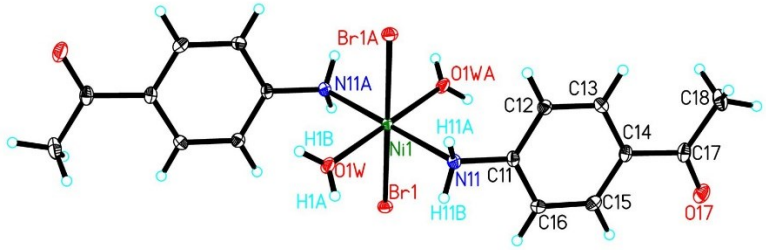

b)

c)

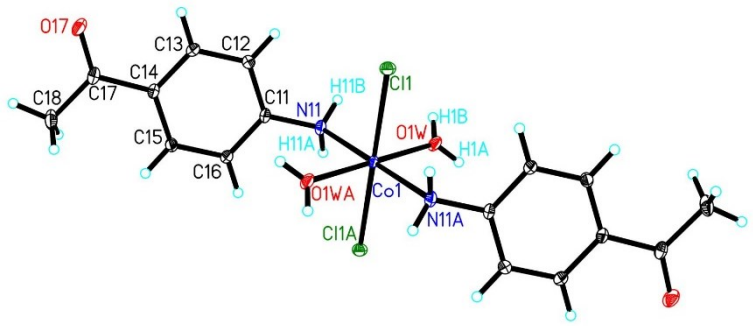

d)

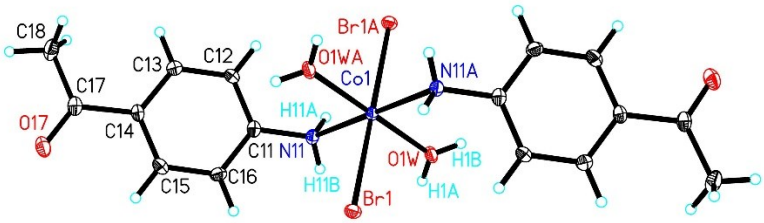

Figure 3: Thermal ellipsoid plots of the molecular units of compound **3**(a), **4**(b), **5**(c), and **6**(d). Only the asymmetric unit, central atom coordination sphere and those hydrogen atoms whose positions were refined, are labeled.

The additional coordination of the two water molecules introduces significant changes in the molecular packing of compound **3**. The molecules are linked into chains parallel to the *a*-axis via pairs of hydrogen bonds between OW1…Cl1A ($d_{(D...A)}$ =3.104(9)) and N11…Cl1a ($d_{(D...A)}$= 3.367(9) [symm. op. A = 2-*x*,-*y*,-*z*]. The chloride ion, OW1 and N11 from one molecular unit H-bond with the chloride ion, OW1, and N11 from an adjacent molecular unit as shown in Figure 4a. The hydrogen bond distances between the coordinated water molecules and chloride ions are ~0.26 Å shorter than the hydrogen bond distances between the nitrogen atom's hydrogen atoms and the chloride ions. The decreased atomic radius of oxygen in comparison with nitrogen is not great enough to make up for the difference in donor-acceptor distances and thus they are stronger. The chains are linked into layers via hydrogen bonds parallel to the *bc*-face (Figure 4b) between O17 and OW1A ($d_{(D...A)}$= 2.717(4)) [symm. op. A = x+1,*y*-*1*,*z*]. These hydrogen bonds

are the strongest interactions in the crystal lattice. The molecular units pack to maximize the number of traditional hydrogen bonds.

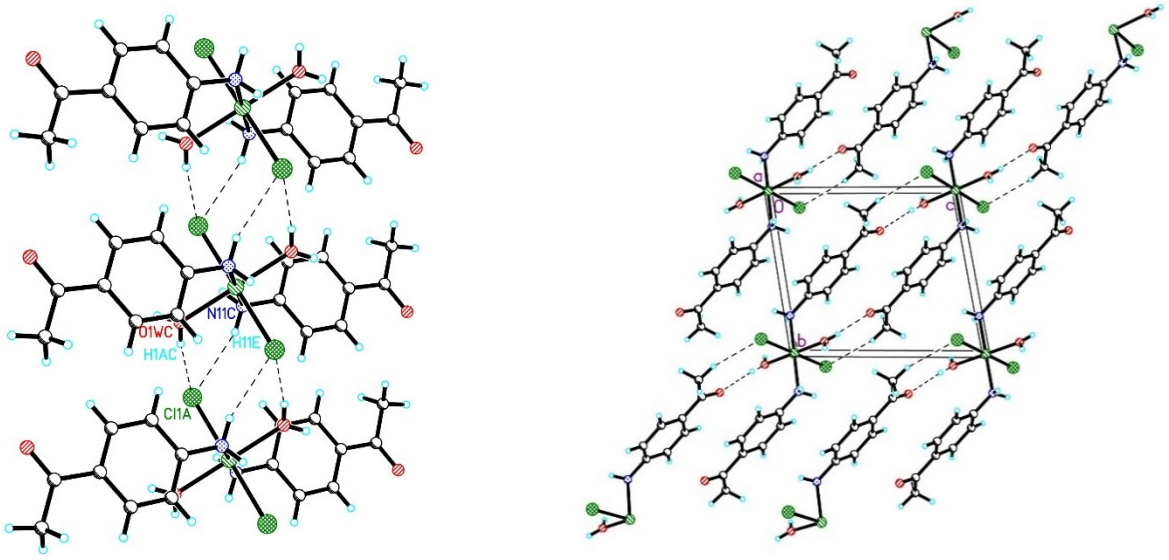

a.) b.)

Figure 4: a) Crystal packing of **3** showing chain formation through H-bonds and b) those chains packing into layers.

There are no significant differences in the crystal packing of compounds **3**-**6**. The slight differences present are a result of the different metal and halide ions and are comparable with the increase in ionic radius of the cobalt ion and bromide ion. Packing diagrams of compounds **4** (S8 and S9), **5** (S11 and S12) and **6** (S14 and S15) are included in the SI. The overall structures are in good agreement with the corresponding nitrate compound, $[Co(4'\text{-}AAP)_2(H_2O)_2(NO_3)_2]$ [75]. Similar hydrogen bonding from the coordinated water molecules to the acetyl oxygen atoms and to the nitrate ions (in place of the chloride ions) are purported, although the hydrogen atoms were not located in the structure.

Compound **7** crystallizes in the monoclinic space group I2/*a* with one chloride ion, one 4'-AAP ligand, and one-half Zn(II) ion comprising the asymmetric unit. Unlike compounds **1**-**6** the Zn(II) ion is not located on a crystallographic inversion center, but rather is on a 2-fold axis. Its coordination sphere contains two chloride ions and two 4'-AAP molecules in a tetrahedral geometry (see Figure 5; a figure showing the asymmetric unit may be found as Figure S16 in the SI). The Zn-N bond length is 2.0542(14) Å, very similar to the Cu-N bond lengths seen in

compounds **1** and **2** and comparable to those seen in other di-aniline complexes with zinc and chloride in the coordination sphere such as $[ZnCl_2(C_6H_7N)_2]$ [76] and $[ZnCl_2(C_6H_6NCl)_2]$ [60]. The N11-Zn1-Cl1 bond angles average 110°, indicating a very slight distortion from tetrahedral geometry. The aromatic ring is virtually planar (mean deviation of constituent atoms= 0.0064Å), with both the carbon atom of the carbonyl substituent (-0.214Å) and N11 atom (0.0657Å) displaced slightly to opposite faces. The carbonyl moiety in this compound is canted slightly in comparison to the plane of the ring; the O17-C17-C14-C15 torsion angle in compound **7** is 9.1°. This torsion angle is significantly greater than observed in compounds **1-6**. The plane of each aromatic ring is inclined (in the same direction) 71.66° away from the N11-Zn1-Cl1 plane. The plane of each aromatic ring is also canted slightly so each ligand is positioned closer to one chloride ion. The C11-N11-Zn(II)-Cl torsion angle is -41.12°, whereas the C11-N11-Zn(II)-ClA torsion angle is 75.27°.

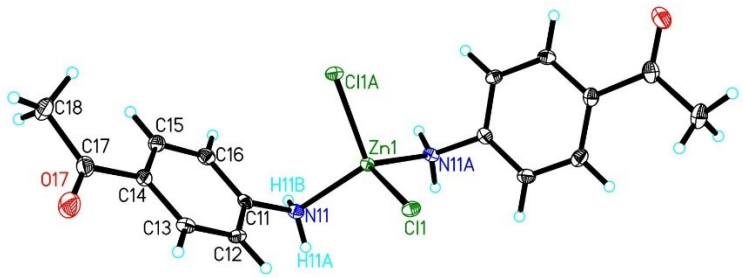

Figure 5: A thermal ellipsoid plot of the molecular unit of **7**. Only the asymmetric unit, Zn(II) coordination sphere and those hydrogen atoms whose positions were refined, are labeled.

The unit-cell translation related molecules are linked into chains parallel to the *b*-axis via two pairs of symmetry equivalent H-bonds between the two chloride ions from one molecular unit and the two amino groups of an adjacent unit (Figure 6a). Although these hydrogen bonds are very weak individually, they work together to generate the chains ($d_{(D...A)}$= 3.423(14) Å) [symm. op. A = *x,y*+1,*z*]. Similar to compounds **1** and **2**, the chains are linked into layers by nontraditional hydrogen bonds parallel to the *c*-axis (Figure 6b). These interactions occur between O17a and hydrogen atoms of C18 ($d_{(D...A)}$= 3.434(11)Å) [symm. transform A = 2-*x,y*+1/2,-*z*+1]) and provide 3D-stabilization of the lattice.

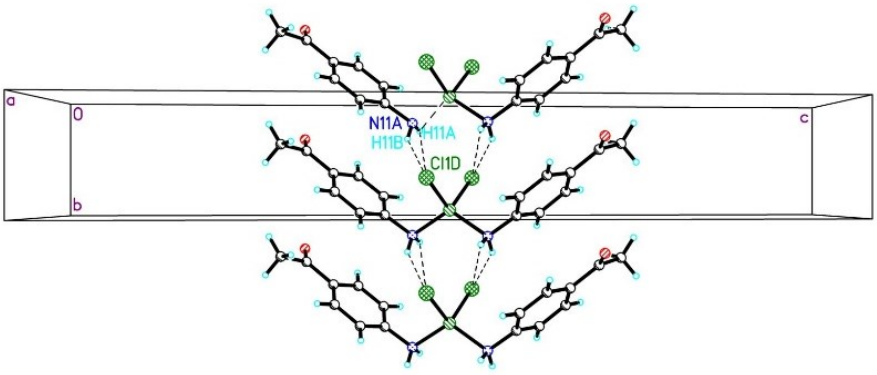

a)

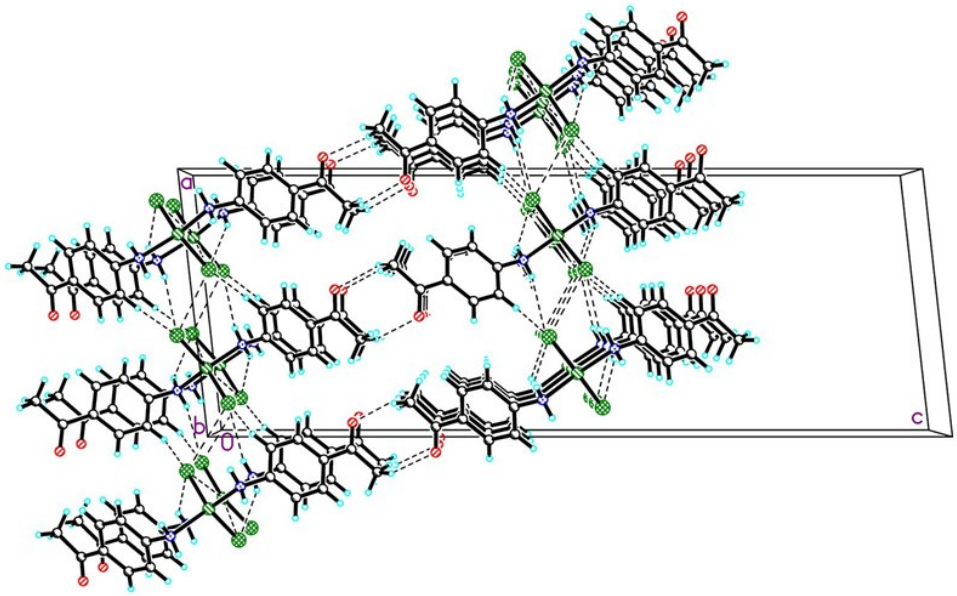

b)

Figure 6: a) Crystal packing of **7** showing H-bond linked chains parallel to *b*-axis and b) H-bond linked layers parallel to the *c*-axis (b).

Compound **8** crystallizes in the monoclinic space group $P2_1/c$. Unlike compound **7,** the Zn(II) ion is not located on a symmetry site. The asymmetric unit comprises one Zn(II) ion, two bromide ions and two 4'-AAP ligands in a tetrahedral geometry (Figure 7). One of the 4'-AAP ligands is two-site disordered with refined occupancies of 0.827(6) and 0.173(5) for the major and minor components, respectively. The Zn1-N11 bond length is 2.068(3)Å which is comparable with the values for compound **7**. The Zn1-Br1 bond length is 2.3617(3), the shortest M1-Br1 bond length of all the compounds discussed which, if they were all tetrahedral complexes, would be somewhat surprising given its larger radius compared to Co, Ni and Cu. However, because zinc is four coordinate, and cobalt and nickel are both six coordinate, they

have larger ionic radii[77] in comparison which explains why the Zn1-Br1 bond length is the shortest. The N11-Zn1-N21 angle is 112.8° and the Br1-Zn1-Br2 angle is 109.64° indicating a slight distortion from tetrahedral geometry. The aromatic ring is virtually planar (mean deviation of constituent atoms= 0.0064Å), with both the carbon atom of the carbonyl substituent (-0.0214Å) and N11 atom (0.0657Å) displaced slightly to opposite faces. The plane of each aromatic ring is inclined towards one another but at slightly different angles. The C11 aromatic ring is inclined 74.20° from the N11-Zn1-Br1 plane whereas the C21 aromatic ring is inclined 70.41° from the N11-Zn1-Br2 plane. The plane of each aromatic ring is canted so the ligand is positioned closer to one bromide ion (Br1 or Br2). The Br1-Zn1-N11-C11 torsion angle is 34.64° and the Br2-Zn1-N11-C11 torsion angle is -82.99° whereas the Br1-Zn1-N21-C11 torsion angle is 29.30° and the Br2-Zn1-N21-C11 torsion angle is -91.41°. The C21 aromatic ring is two-site disordered. The refined occupancies show distinct major (82.7%) and minor (17.3%) components. A figure including the disordered ring is shown in Figure S17 in the SI.

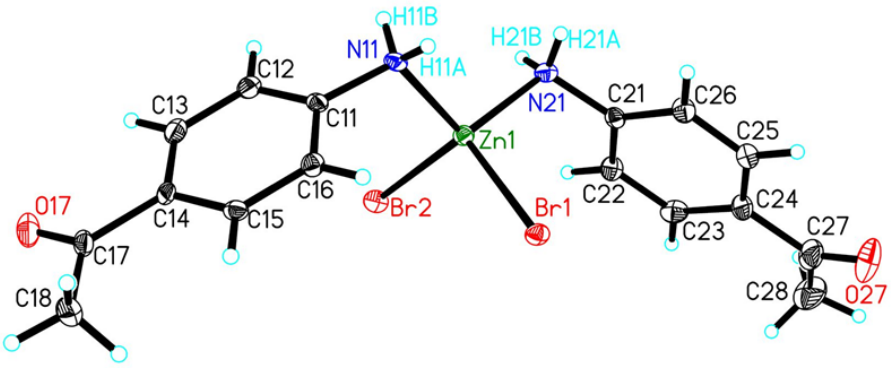

Figure 7: A thermal ellipsoid plot of the molecular unit of **8**. Only those hydrogen atoms whose positions were refined are labeled. Only the major component of the disordered C21 ring is shown for clarity

The unit-cell translation related molecules are linked into chains parallel to the *a*-axis through a series of H-bonds (Figure 8a). The Br1 of each molecular unit forms H-bonds with both N11 and N21 amino groups of an adjacent unit ($d_{(D\ldots A)}$= 3.56(6) Å) [symm. op. *a=x+1,y,z*]. The Br2 ion of each molecular unit forms a single H-bond ($d_{(D\ldots A)}$= 3.43(6) Å) with the same N11 amino group to which Br1 H-bonds. The Br2 ion of each molecule also forms short Br…Zn1 contacts with the adjacent unit, with a Br2..Zn1 distance of 3.92(7) Å. The chains are linked via hydrogen bonds and short halide-halide contacts in an alternating pattern to form layers parallel to the *bc* plane (Figure 8b). This disorder in the N21 ring introduces significant

change in the way in which these molecular units pack together because the carbonyl of the disordered ring is less available for hydrogen bonding. The H-bonds occur between the N21 of one molecular unit and the O17 of a non-parallel adjacent unit along the *bc* face diagonal ($d_{(D...A)}$= 2.963(14) Å) [symm. op. *a= x, 1-y, 1-z*]. These H-bonds are further stabilized by non-traditional H-bonds between the Br2 and the C18 hydrogen atoms from a non-parallel adjacent unit ($d_{(D...A)}$= 3.681(14) Å). There are short Br…Br contacts that link pairs of parallel chains into dimers. The Br1…Br1a distance is 4.005Å, Zn1-Br1…Br1a angle is 118.76, and the Zn1-Br1…Br1a-Zn1a torsion angle is 180°. The disordered rings are located in a cavity and the O17 of this ring does not participate in any hydrogen bonding which explains the alternating pattern of the chains.

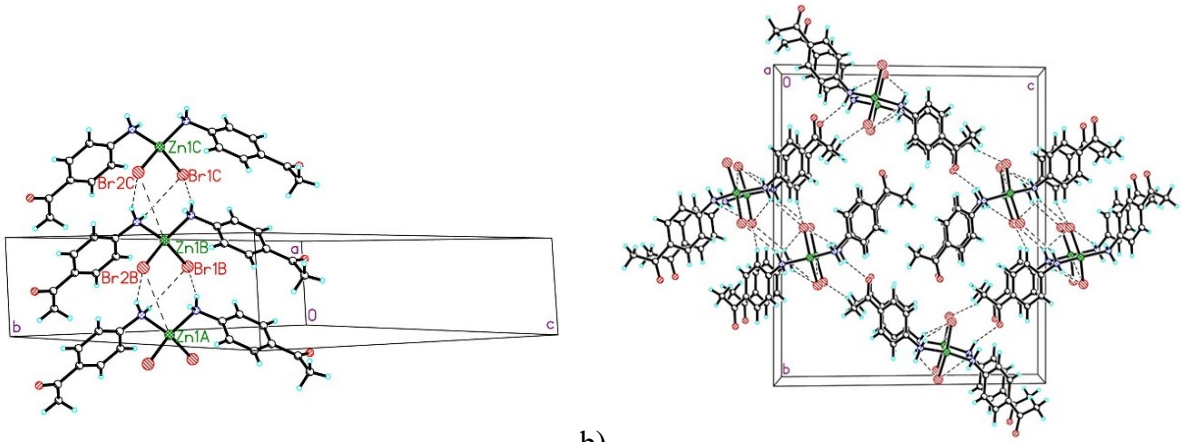

a) b)

Figure 8: Crystal packing of compound **8** .) highlighting H-bond linked chains parallel to a-axis and b) highlighting H-bonded alternating chains linked to form layers.

3.1 IR spectra

The most notable aspects of the IR spectra are observed in the absorptions from the NH_2 group and carbonyl group upon coordination of the ligands. The free ligand shows broad absorbances for the symmetric and anti-symmetric N-H stretching vibrations at 3390 and 3328 cm^{-1}. The absorbances for the N-H stretching vibration in the anhydrous products (**1, 2, 7, 8**) are much sharper, indicating weaker H-bonding upon coordination, but also appear at lower energy (3302 and 3217 cm^{-1}), demonstrating the change in hybridization upon coordination ($sp^2 \rightarrow sp^3$).

The absorbances for the N-H stretching vibrations in the di-hydrated products (**3-6**) are overlapped by the O-H stretching vibrations of the water molecules so they appear broad. Similar to the anhydrous products, the N-H absorbances moved to lower energy (3318 and 3232 cm^{-1}).

The free ligand shows a sharp, intense band at 1652 cm^{-1} that is the absorbance of the carbonyl. In all compounds **1-8** the absorbance for the carbonyl moves to higher energy suggesting a decrease in the hydrogen bond strength. In the anhydrous products, the absorbance appears near 1682cm^{-1} and in the di-hydrated products it appears near 1662 cm^{-1}.

3.4. Magnetic Properties

Magnetization. Magnetization data as a function of field for compounds **1-6** were collected at 1.8K and are shown in the SI as Figures S18-S23 respectively. The moments of compounds **1** and **2** reach ~ 110 and 125 emu/mol at 10 kOe, respectively, values well below the expected saturation value of ~ 6,000 emu/mol for S = ½ and g slightly greater than 2. This indicates the presence of antiferromagnetic interactions in the samples. Further, upward curvature is observed in M(H) for both compounds indicating the presence of a low-dimensional magnetic lattice [78]. Compounds **3**-**6** reach values of ~ 3500, 4100, 9000, and 7800 emu/mole, respectively, also well below the expected saturation values of ~ 12,000 for S = 1 and 17,000 emu/mol for S = 3/2. However, this is not necessarily indicative of antiferromagnetic exchange for these ions as both exhibit single-ion anisotropy leading to reduced moments and temperature dependence in the absence of interactions [78].

Susceptibility (χ) and χT as a function of temperature (0-310 K) in an applied field of 1 kOe for **1** are shown in Figure 9. The appearance of a maximum in χ near 10 K indicated the presence of antiferromagnetic exchange in the material. Initial attempts to fit the data to the 1D-Heisenberg chain model gave poor results. The data were then fit to the 1D-Heisenberg chain model incorporating a Curie-Weiss correction for interchain interactions which provided good agreement. Results for the fits to both χ(T) and χT(T) are shown in Table 4. The data for **2** were qualitatively similar and treated in the same fashion (see Figure 10 and Table 4). For **2**, a slight paramagnetic tail was seen at the lowest temperatures which was well modeled as ~ 2.3% paramagnetic impurity.

Table 4

Fitted magnetic parameters for **1**-**6**

	Model	**CC** (emu-K/mol Oe)	**J/k_B** (K)	**θ** (K)	**D** (K)	**p** (%)
1 χ(T) χT(T)	1D-Heis. S = ½ wCW	0.436(3) 0.430(1)	-13.5(5) -13.3(6)	-4.3(6) -4.0(5)		1.6(1) 1.2(1)
2 χ(T) χT(T)	1D-Heis. S = ½ wCW	0.444(1) 0.431(1)	-14.2(3) -14.4(4)	-2.96(6) -2.1 (3)		2.38(7) 2.3(2)
3	CW Law χT(T) SIA	1.224(8) 1.212(1)		-0.58(7) -0.18(3)	8.6(1)	
4	CW Law χT(T) SIA	1.056(9) 1.05(1)		-0.24(9) -0.17(3)	5.3(1)	
5	CW Law (to 50 K) χT(T) SIA	2.72(1) 2.72		-4.3(4) -0.25(2)	40(2)	
6	CW Law (to 50 K) χT(T) SIA	2.59(1) 2.59		-4.3(3) -0.27(2)	54(2)	

CC = Curie constant, J = magnetic exchange, θ = Weiss constant, D = single-ion anistropy, p = percent paramagnetic purity, 1D-Heis = one-dimensional Heisenberg model, CW = Curie-Weiss, SIA = single-ion anisotropy model.

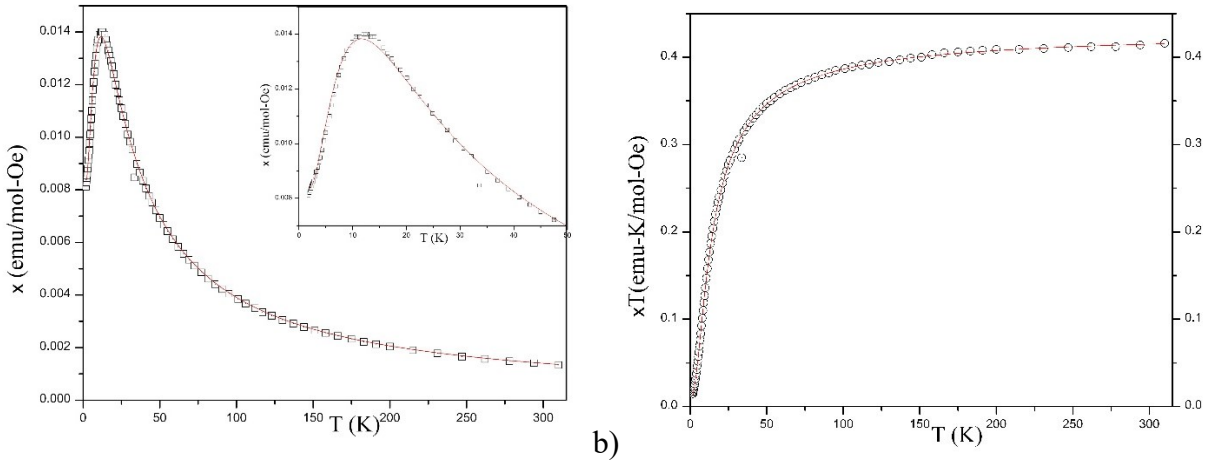

a) b)

Figure 9. a) χ(T) for **1**. The inset shows an expansion of the region near the maximum in χ. b) χT(T) for **1**. The solid lines show the best fits to the 1D-Heisenberg chain model.

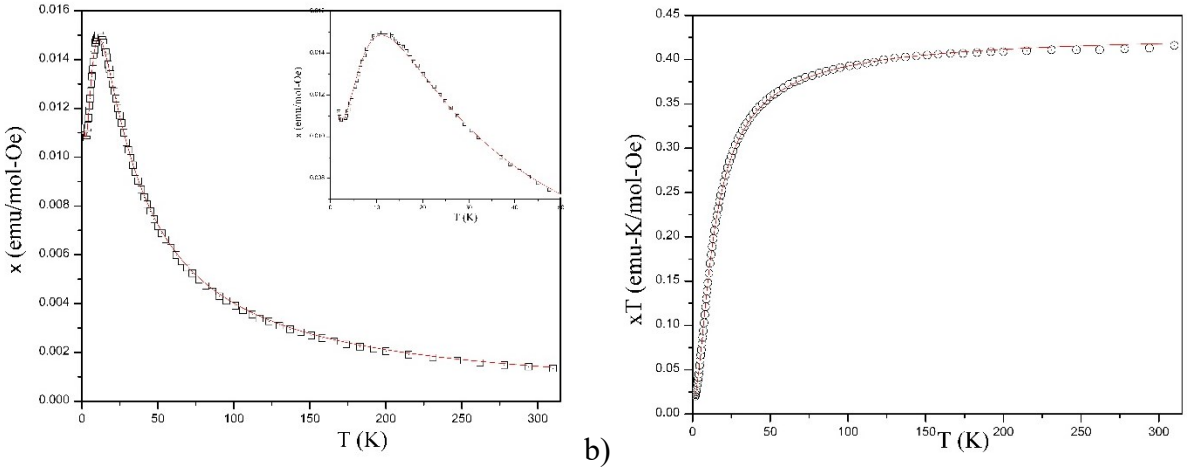

a) b)

Figure 10. a) χ(T) for **2**. The inset shows an expansion of the region near the maximum in χ. b) χT(T) for **2**. The solid lines show the best fits to the 1D-Heisenberg chain model.

Similarly, susceptibility as a function of temperature data were collected for the nickel compounds **3** and **4.** For both compounds, χ rises monotonically with decreasing temperature; no maxima are observed (see Figures S24 and S25 in the SI). The data were initially fit to the Curie-Weiss Law giving good quality fits (see Figure 11) with Weiss constants near zero (-0.2 to -0.6 K, see Table 4). Plots of χT(T) show little temperature dependence down to ~ 20 K, followed by a sharp decrease at lower temperatures. Given the limited superexchange pathways and the well-established single-ion anistropy (SIA) of the S = 1 system, the data were fit to a single-ion anisotropy model for an S = 1 system with a Curie-Weiss correction to account for potential intermolecular interactions. The data fit the model excellently (see Figure 11) yielding Curie constants in good agreement with the values obtained from the Curie-Weiss plots and small values for the Curie-Weiss corrections, supporting a minimal contribution from intermolecular magnetic interactions.

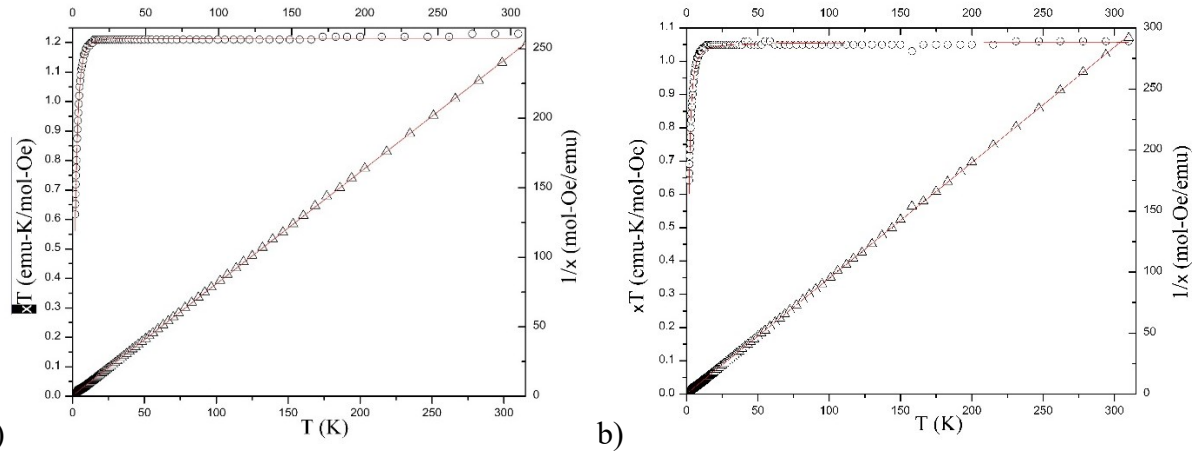

a) b)

Figure 11: χT(T) (o, left axis) and 1/χ (T) (Δ, right axis) for **3** (a) and **4** (b).

The cobalt compounds, **5** and **6**, also exhibit temperature temperature dependence which can be attributed primarily, but not solely, to SIA. Curie-Weiss plots (Figures S26 and S27 respectively) provide good estimates of the Curie Constant, but due to the strong anisotropy of the Co(II) ions, the value of θ is not a valid measure of the potential for magnetic interactions within the samples. For both compounds, χ rises monotonically with decreasing temperature (Figure 12) with no indication of a maximum. Plots of χT(T) show significant decreases below ~100 K, indicative of SIA, antiferromagnetic exchange, or both.

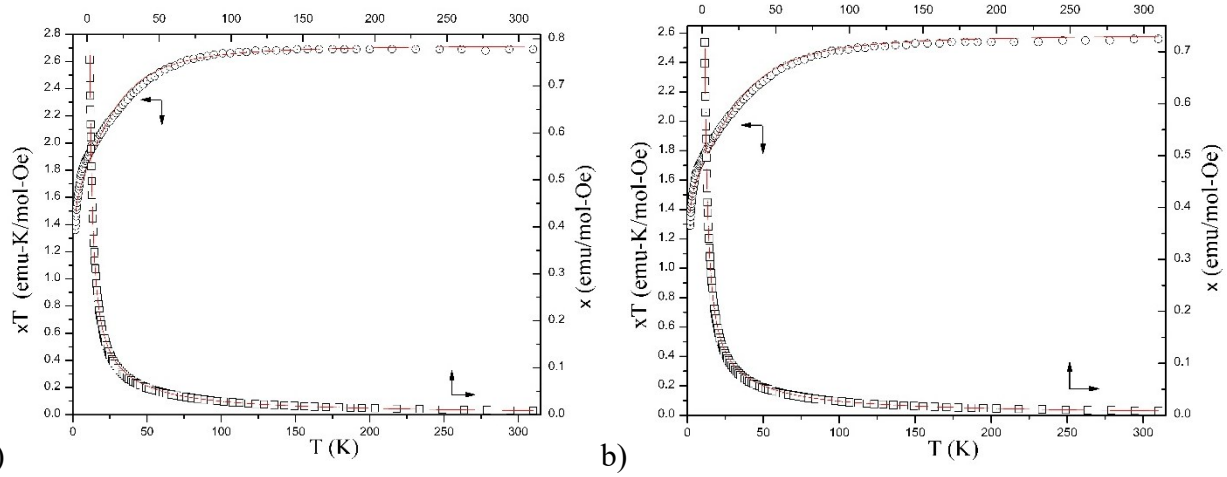

a) b)

Figure 12: χ(T) (□, left axis) and χT(T) (o, right axis) for **5** (a) and **6** (b). Note that the temperature axis is offset for the χ(T) data (top axis) for clarity at low temperatures.

As indicated previously [79], the χT product for an octahedral Co(II) ion exhibits SIA with a low temperature limit near 1.7 emu-K/mol-Oe in the absence of any exchange. An examination of Figure 12 shows that the χT product is indeed approaching that value with decreasing temperature until ~4 K, whereupon a further down turn occurs. Taking this additional decrease as a sign of possible antiferromagnetic interactions, the data for **5** and **6** were fit to the model for an isolated S = 3/2 ion using the Curie constant obtained from the Curie-Weiss fit with an added Curie-Weiss correction for possible intermolecular interactions. The results (solid lines in Figure 12, Table 4) indicate that the temperature dependence is primarily SIA, with a minor contribution from antiferromagnetic exchange ($\theta < 0$).

4. Discussion

Six of the eight compounds (**1-6**) crystallize in the triclinic space group *P*-1 whereas the other two compounds crystallize in monoclinic space groups *I*2/*a* (compound **7**) and $P2_1/c$ (compound **8**). Compounds **1, 2, 7,** and **8** each have the general formula L_2MX_2 and have either slightly distorted square planar (**1** and **2**) or slightly distorted tetrahedral (**7** and **8**) geometry. Compounds **3-6** follow a general pattern of nearly octahedral geometry with the additional coordination sites occupied by water molecules. In compounds **1-6** the metal ion lies on an inversion center. The anhydrous compounds have slightly shorter M-X and M-N11 bonds lengths than the dihydrate compounds. The N11-C11 bond length is very similar in all eight compounds.

Compounds **1**-**8** all form chains parallel to the *a*-axis (**1-6, 8**) or *b*-axis (**7**) via four distinct systems of intermolecular interactions. Compounds **1** and **2** are isostructural. These compounds form chains through bihalide interactions that are linked into layers through non-traditional hydrogen bonds and halogen bonds (with the potential for antiferromagnetic exchange via the two-halide pathway [74]. For the two-halide interactions in these two compounds, the noteworthy interaction distances and angles are comparable to one another within the error. In compound **1** the Cl1…Cl1a distances (~3.7 Å) are about 0.1 Å shorter than those observed in the bromide complex **2** (~3.8 Å) as would be expected given the smaller radius of the chloride ion. The non-traditional hydrogen bonding between adjacent molecules that links the chains into layers mirrors the differences seen in the two-halide interactions. The D…A distances are slightly shorter (~0.03 Å) for the chloride complexes than for the bromide complexes.

Compounds **3-6** are linked into chains through pairs of H-bonds, which are further linked into layers through both traditional and non-traditional H-bonds. There are differences between the metal chloride compounds (**3,5**) and the bromide complexes (**4,6**) as expected due to the increased ionic radius of the bromide ion. In the chloride complexes, the D..A distance for both the OW1-X1a and N11-X1a hydrogen bonds is shorter (~0.15 Å, ~0.1 Å, respectively) than those observed in the bromide complexes. As mentioned previously, the H-bonds between the coordinated water molecules and the halide ions are consistently stronger (~8-10% based on distance) than the H-bonds between the nitrogen hydrogen atoms and the halide ions. The traditional hydrogen bonds between the carbonyl oxygen atoms and the coordinated water molecules are the strongest intermolecular interactions within the entire crystal lattice for all four compounds, with a D…A distance ~0.3 Å shorter than the hydrogen bonds between the coordinated water molecules and the halide ions. The D…A distance for the H-bonds between the carbonyl oxygen atoms and the coordinated water molecules in compounds **3**-**6** remain within 0.04 Å of one another, with compound **4** having the longest D…A distance (2.7298(19) Å). H-bonds between halide ions and methyl hydrogen atoms are also observed ($d_{(D...A)}$ ~3.8) , which supplement the organization of the chains into layers. In the metal bromide compounds (**4,6**), very weak non-traditional hydrogen bonds are found between the bromide ions and aromatic hydrogen atoms with a D…A distance of ~3.86 Å. These nontraditional hydrogen bonds are not observed in the metal chloride compounds, likely because of the decreased ionic radius of the chloride ions making the interspecies distances too great for any significant interaction.

Compounds **7** and **8** are isostructural, but not isomorphous, and each have distorted tetrahedral geometry. Both compounds pack into chains in a similar fashion but the formation of the layers from those chains occurs in a slightly different way at least in part due to the disorder in one of the aromatic rings of compound **8**. Although the chains pack together in a similar fashion, compound **7** forms four hydrogen bonds between adjacent molecular units in the chain, whereas compound **8** only forms three hydrogen bonds between adjacent units within the chain.

Compound **7** forms chains through two pairs of hydrogen bonds between the hydrogen atoms of each amino-nitrogen and the chloride ions. One H-bond in each pair has a D…A distance ~0.1 Å shorter than the other H-bond in the pair. Compound **8** forms one pair of H-bonds between one hydrogen atom from each nitrogen atom and one of the bromide ions (Br1).

The second hydrogen atom on N11 forms a hydrogen bond to the other bromide ion (Br2). All three of these hydrogen bonds are very similar to the pairs of H-bonds in compound **7**, but the D…A distances of the bromide complex are ~0.15 Å longer. The hydrogen atom on N21 that is not involved in hydrogen bonding within the packing of the chain links chains together along the *bc*-face diagonal through hydrogen bonds with the carbonyl oxygen atoms. These are the strongest interactions within the crystal lattice, with a D…A distance of 2.963(4) Å. In compound **7**, the chains are linked into layers through two-halide interactions and nontraditional H-bonds between the carbonyl oxygen atom and methyl hydrogens. Adjacent chains are oriented in opposite directions with Cl1-Zn-Cl1 aligned up or down relative to one another. In compound **8**, pairs of parallel chains are linked into dimers through two halide interactions. Similar to compound **7**, the pairs of parallel chains are oriented in opposite directions, with Br1-Zn-Br2 units in adjacent chains aligned up or down relative to each other. The chains in compound **8** are further linked through a system of very weak traditional and nontraditional hydrogen bonds (Table 3). Unfortunately, because these compounds are not isostructural with the other six compounds, they cannot serve as a diamagnetic analogue for comparison.

Due to the difference in coordination number between compounds **1, 2, 7, 8** and **3-6**, the packing of these compounds into a 3D crystal lattice occurs in different ways. In compounds **3-6** there are no two-halide or bihalide interactions stabilizing the crystal lattice. The packing of these compounds is completely dependent on hydrogen bonds. Compounds **1** and **2** have the same coordination number as **7** and **8** but different geometries (square planar and tetrahedral, respectively). Not surprisingly, this causes differences in the crystal packing. In compounds **1** and **2**, the units are linked into chains through bihalide interactions whereas in compounds **7** and **8** the units are linked into chains through traditional hydrogen bonds. Compounds **1** and **2** pack into chains that are all oriented in the same direction whereas compounds **7** and **8** pack into chains where adjacent chains are oriented in opposite directions. In compounds **1,2** and **7** the chains are linked into layers through short halide-halide contacts and nontraditional hydrogen bonds. In compound **8**, similar interactions are present, but the disorder causes the interactions to appear in slightly different ways. The disorder in compound **8** prevents the carbonyl oxygen atom in the disordered ring from serving as a strong H-bond acceptor, thus preventing it from forming any hydrogen bonds. In compounds **1,2**, and **7**, the bihalide and two halide interactions are supported by non-traditional hydrogen bonds between the carbonyl oxygen atom and the

methyl hydrogens. Without both carbonyl oxygen atoms able to form supporting hydrogen bonds, the short halide-halide contacts in compound **8** appear less frequently and in a different way.

The difference in coordination number, geometry, and the identity of the metal ion each have a significant effect on the non-bonded interactions and packing of the crystal structure. These effects either restrict or induce super exchange pathways which could propagate antiferromagnetic or ferromagnetic interactions within the materials. Compounds **1** and **2** each exhibit short enough metal-halide and halide-halide contacts that bihalide and two-halide mediated superexchange is possible. Steric hindrance caused by the additional coordination of the two water molecules in compounds **3-6** prevents the formation of short metal-halide or halide-halide contacts and eliminates the bihalide or two-halide pathways for those compounds.

The Cu(II) compounds, **1** and **2**, exhibit significant antiferromagnetic interactions with maxima in χ near 12 K. The copper ions are linked in chains via bihalide bridges parallel to *a*-axis and via the two-halide pathway parallel to the *b*-axis. This suggested a uniform chain model with the possibility of significant interactions between the chains, that the data are well fitted in that form. However, the fitting cannot indicate which is the primary exchange interaction – parallel to the *a*- or *b*-axis. Future theoretical calculations may be able to distinguish those superexchange pathways. The Ni(II) and Co(II) complexes all show magnetic behavior driven by the single-ion anisotropy of the S = 1 and S = 3/2 ions respectively. Fitting suggests very weak antiferromagnetic exchange between the molecules via non-zero Weiss constants, but the model is crude and more definitive interpretation of the data must await a more sophisticated analytical expression or the use of techniques such as Monte Carlo simulations.

5. Conclusion

Two families of compounds have been prepared using 4'-aminoacetophenone. These families of compounds have coordination numbers of four and six. The family of compounds with the coordination number of four crystallize in a variety of space groups and have either square planar or tetrahedral geometry. These compounds form linear chains either through hydrogen bonding or bihalide interactions, which form layers through two halide interactions and non-traditional hydrogen bonding. The copper compounds show weak antiferromagnetic exchange, while the zinc compounds serve as diamagnetic analogues. The family of compounds with the coordination number of six all crystallize in the triclinic space group P-1 and are isostructural.

These compounds form both chains and layers through hydrogen bonding. The nickel compounds are paramagnetic with a temperature dependent moment due to SIA. The cobalt compounds show both SIA and weak antiferromagnetic exchange. The incorporation of a strong electron withdrawing ketone in the para position of the aniline-based ligand in these families of compounds begins to fill a hole in our collective knowledge. Although the ketone didn't affect the coordination of the nitrogen, it played a significant role in hydrogen bonding and layer formation. Further work is in progress, including preparation and analysis of a family of salt complexes with the same organic component.

Acknowledgments: LM is grateful for financial support from SEQENS through a summer undergraduate fellowship. We are grateful for funds from SEQENS toward the purchase of the D8 Focus diffractometer, from the National Science Foundation (IMR-0314773) for purchase of the MPMS SQUID magnetometer, and from the Kresge Foundation toward the purchase of both. In addition, we are grateful for funding from the NSF (CHE-2018870) toward the purchase of the PhotonIII diffractometer (U. Virginia).

Supplementary Information:
CCDC 2211686-2211693 contain the supplementary crystallographic data for **1**-**8** respectively. These data can be obtained free of charge via https://www.ccdc.cam.ac.uk/structures/, or from the Cambridge Crystallographic Data Centre, 12 Union Road, Cambridge CB2 1EZ, UK; fax: (+44) 1223-336-033; or e-mail: deposit@ccdc.cam.ac.uk.
Figures showing the asymmetric units of compounds **1**-**8** (Figures S1, S2, S6, S7, S10, S13, S16, S17, respectively); the packing structure of **2** (S3-S5), **4** (S8, S9), **5** (S11, S12) and **6** (S14, S15); M(H) plots for **1-6** (S18-S23); χ(T) plots for **3** (S24) and **4** (S25); Curie-Weiss plots for **5** (S26) and **6** (S27).

References

1. G. Christou, D. Gatteschi, D.N. Hendrickson, R. Sessoli. MRS Bulletin, 25, (2000) 66.
2. D.N. Woodruff, R.E.P. Winpenny, R.A. Layfield Chem. Rev. 113 (2013) 5110.
3. A. Zabala-Lekuona, J.M. Seco, E. Colacio Coord. Chem. Rev.-441 (2021) 213984.
4. M. Ferbinteanu, H. Miyasaka, W. Wernsdorfer, K. Nakata, K. Sugiura, M. Yamashita, C. Coulon, R. Clérac J. Am. Chem. Soc. 127 (2005) 3090.
5. K. Bernot, L. Bogani, A. Caneschi, D. Gatteschi, R. Sessoli J. Am. Chem. Soc. 128 (2006) 24, 7947.
6. C. Coulon, H. Miyasaka, R. Clérac Single-Molecule Magnets and Related Phenomena, pp 163–206 in Winpenny, R. (ed) Single-Molecule Magnets and Related Phenomena. Structure and Bonding, vol 122. Springer, Berlin, Heidelberg.

7. G.A. Craig, M. Murrie Chem. Soc. Rev. 44 (2015) 2135.
8. Y.-S. Meng, S.-D. Jiang, B.-W. Wang, S. Gao Acc. Chem. Res. 49 (2016) 2381.
9. Min Feng and Ml Tong Chemistry - Eur. J. 24 (2015) 757.
10. P. Yang, H. Hu, S. Yu, D. Liu, Y. Liang, H. Zou, F. Liang, Z. Chen, Inorg. Chem., 60 (2021) 14752.
11. E. Garlatti, A. Chiesa, P. Bonfa, E. Macaluso, I.J. Onuorah, V.S. Parmar, Y.-S. Ding, Y.-Z. Zheng, M.J. Giansiracusa, D. Reta, E. Pavarini, T. Guidi, D.P. Mills, N.F. Chilton, R.E.P. Winpenny, Richard P. Santini, S. Carretta, J. Phys. Chem. Letters, 12 (2021) 8826.
12. H. Li, L. Xi, P. Jing, J. Tang, Q. Wang, H. Yang, L. Zhai, Y. Niu, L. Ding, Z. Song, J. Mater. Chem. C, 9 (2021) 294.
13. J.-H. Wang, Z.-Y. Li, M. Yamashita, X.-H. Bu, Coord. Chem. Rev, 428 (2021) 213617.
14. K. Son, R.K. Kim, S. Kim, G. Schuetz, K.M Choi, H. Oh, Phys. Status Solidi A, 217 (2020) 1901000.
15. JJ. Lai, Z.-Y. Ruan, G.-Z. Huang, J.-L. Liu, M.-L. Tong, Inorg. Chem. Comm., 132 (2021) 108807.
16. M. Cirulli, E. Salvadori, Z.-H Zhang, M. Dommett, F. Tuna, H. Bamberger, J.E.M. Lewis, A. Kaur, G.J. Tizzard, J. van Slageren, R. Crespo-Otero, S.M. Goldup, M.M. Roessler, Angew. Chem., Int. Ed., 60 (2021) 16051.
17. S.G. McAdams, A.-M. Ariciu, A.K. Kostopoulos, J.P.S. Walsh, F. Tuna, Coord. Chem. Rev., 346 (2017) 216.
18. A.V. Pavlischuk, V.V. Pavlischuk, Theor. Exp. Chem., 57 (2013) 163.
19. Y. Wang, Z. Wang, J. Yang, X. Li, J. Phys. Chem. Lett., 11 (2020) 9819.
20. D. Luneau, Euro. J. Inorg. Chem., 2020 (2020) 597.
21. W. Lan, Z. Zhou, J. Li, Y. Dou, X. Hao, L. Yang, H. Liu, D. Li, Q. Liu, D. Zhang, Acta Crystallogr. C., 75 (2019) 1475.
22. M.A. Al-Azzani, F. Al-Mjeni, R. Mitsuhashi, M. Mikuriya, I.A. Al-Omari, C. C. Roberstson, E. Bill, M. S. Shongwe, Eur. J. Chem., 26 (2020) 4766.
23. C. Yang, Y.-H. Wei, S. Xu, H.-Y. Zhang, Y.-Q. Yang, B. Zhang, M. Fang, New J. Chem., 45 (2021) 14103.
24. M.J. Daum, A. Ramanathan, A.I. Kolesnikov, S. Calder, M. Mourigal, H.S. La Pierre, Phys. Rev. B, 103 (2020) L121109.
25. Z. Zhu, M. Guo, X.-L. Li, J. Tang, Coord. Chem. Rev., 378 (2019) 350.
26. J.-H. Liu, R.-T. Zhang, J. Zhang, D. Zhao, X.-X. Li, Y.-Q. Sun, S.-T. Zheng, Inorg. Chem., 58 (2019) 14734.
27. Y. Huo, Y.-C. Chen, S.-G. Wu, J.-L. Liu, J.-H. Jia, W.-B. Chen, B.-L. Wang, Y.-Q. Zhang, M.-L. Tong, Inorg. Chem., 58 (2019) 1301.
28. M. Stuckart, M. V. Izarova, M. Glob, J. Klose, C. Schmitz-Antoniak, P. Kogerler, B. Kersting, K. Y. Monakhov, Inorg. Chem., 60 (2020) 8437.
29. Z. Weng, Y. Ren, M. Gu, H. He, Dalton Trans., 47 (2018) 233.
30. J. Lopez- Cabrelles, S. Manas-Valero, I. J. Vitorica-Yrezabal, M. Siskins, M. Lee, P. G. Steeneken, H. S. J. van der Zant, G. M. Espallargas, E. Coronado, J. Am. Chem. Soc., 143 (2021) 18502.
31. A. E. Thorarinsdottir, T. D. Harris, Chem. Rev., 120 (2020) 8716.
32. S.-S. Chen, S.-S Han, C.-B. Ma, W.-D. Li, Y. Zhao, Cryst. Growth Des., 21 (2021) 869.
33. L.C.J.M. Peters, H. Engelkamp, U. Zeitler, P.C.M Christianen, P. Tinnemans, J.-K. Maan, A.E. Rowan, Euro. J. Inorg. Chem., 2021 (2021) 2611.

34. J. Chalupsky, M. Srnec, J. Phys. Chem. A., 125 (2021) 2276.
35. H.-S. Wang, K. Zhang, Y. Song, Z.-Q. Pan, Inorganica Chim. Acta, 521 (2021) 120318.
36. Y. Zhang, K. L. Harriman, G. Brunet, A. Pialat, B. Gabidullin, M. Muralee, Eur. J. Inorg. Chem., 2018 (2018) 1212.
37. A. Biswas, N.A. Zarkevich, Y. Mudryk, A.K. Pathak, A.V. Smirnov, V.P. Balema, D.D. Johnson, V.K. Pecharsky, J. Appl. Phys., 129 (2021) 193901.
38. D.J. Garcia, V. Vildosola, P.S. Cornaglia, J. Phys. Condens. Matter, 32 (2020) 285803.
39. H. Li, P. Jing, J, Lu, X. Lu, Q. Wang, L. Ding, W.-M. Wang, Z. Song, Dalton Trans., 50 (2021) 2854.
40. M.-H. Whangbo, H.-J. Koo, R.-K. Kremer, Molecules, 26 (2021) 531
41. D. Nandy, D. B. K. Chu, D. R. Harper, C. Duan, N, Arunachalam, y. Cytter, H. J. Julik, Phys. Che. Chem. Phys., 22 (2020) 1463.
42. Y. Liu, W. Zhou, G. Tang, C. Yang, X. Wang, J. Hong, J. Phys. Chem. C, 123 (2019) 28919.
43. C.M. Legendre, R. Herbst-Irmer, D. Stalke, Inorg. Chem., 60 (2021) 13982.
44. V.I. Minkin, A.A. Starikova, M.G. Chegerev, A.G. Starikov, Russ. Chem. Bull., 70 (2019) 811.
45. K.H. Sugiyarto, C. Budimarwanti, H.A. Goodwin, Chiang Mai J. Sci., 47 (2020) 1068.
46. Md. Ehesan Ali, S.N. Datta, J. Mol. Struc., 775 (2006) 19.
47. J.-P. Zhao, Y. Xie, J.-R. Li, X.-H. Bu, Dalton Trans., 45 (2016) 1514.
48. X. Shen, H. Zhou, J. Yan, Y. Li, H. Zhou, Inorg. Chem., 53 (2014) 116.
49. P. Agarwal, A. Kumar, I. Verma, R. R. Erande, J. Klak, A.J. Mota, H. Arora, A. Rajput, Now J. Chem., 45 (2021) 1203.
50. Y. Meng, Q.-Q. Sheng, M.N. Hoque, Y.-C. Chen, SG. Wu, J. Tucek, R. Zboril, T. Liu, Z.-P. Ni, M.-L. Tong, J. Euro. Chem. A, 23 (2017) 10034.
51. M. Katsuhara, T. Mori, J. Phys. Soc. of Japan, 73 (2004) 3335.
52. A.D. Richardson, T. J. Zirkman, M. T. Kebede, C. P. Landee, M. Rademeyer, M. M. Turnbull, Polyhedron, 147 (2018) 106.
53. I. Kaljurand, R. Lilleorg, A. Murumaa, M. Mishima, P. Burk, I. Koppel, I.A. Koppel, I. Leito, J. Phys. Org. Chem., 26 (2013) 171.
54. M.L. Schneider, A.W. Markwell-Heys, O.M. Linder-Patton, W.M. Bloch, Front. Chem., 9 (2021) 696081.
55. A. Krogul, J. Skupinska, G. Litwinienko, J. Mol. Catal. A. Chem., 385 (2014) 141.
56. L.A. Koerte, S. Blomeyer, S. Heidemeyer, A. Mix, B. Neumann, N.W. Mitzel, Chem. Comm., 52 (2016) 9949.
57. T. Voss, T. Mahdi, E. Otten, R. Froehlich, G. Kehr, D.W. Stephan, G. Erker, Gerhard, Organometallics, 31 (2012) 2367.
58. S.V.J. Lakshman, J.L. Rao, Indian J. of Pure and Appl. Phys., 10 (1972) 497.
59. G.T. Tigineh, LK. Liu, J. Chinese Chem. Soc., 61 (2014) 1180.
60. J.E. Chellali, C. Keely, G. Bell, K.L. Dimanno, T. Tran, C.P. Landee, D.A. Dickie, M. Rademeyer, M.M. Turnbull, F. Xiao, Polyhedron, 168 (2019) 1.
61. T. Bardakci, A. Altun, K. Golcuk, M. Kumru,. J. Mol. Struct., 1100 (2015) 475.
62. N. Kupko, K.L. Meehan, F.E. Witkos, H. Hutcheson, J.C. Monroe, C.P. Landee, D.A. Dickie, M.M. Turnbull, Polyhedron, 187 (2020) 114680.
63. K.L. Meehan, D. FA Fontaine, A.D. Richardson, S.M. Fowles, B.Mukda, J.C. Monroe, C.P. Landee, D.A. Dickie, M.M. Turnbull, S. Jiang, F. Xiao, Polyhedron, 200 (2021) 115094.
64. R.L. Carlin, Magnetochemistry, Springer-Verlag, Berlin, 1986.

65. Bruker AXS Inc., Madison, WI, USA, (2012)
66. G.M. Sheldrick, Acta Cryst. A 64 (2008) 112.
67. G.M. Sheldrick, Acta Cryst. C71 (2015) 3.
68. We note that a room temperature structure of compound **1** with an R_1 value of 0.0868 has been recently reported. V.Nemec, K.Lisac, M.Liovic, I.Brekalo, D.Cincic, Materials 13 (2020) 2385.
69. G.P. Guedes, F.F. Farias, M.A. Novak, F.L. de A. Machado, M.G.F. Vaz, Inorg. Chim. Acta, 378 (2011) 134.
70. K.R. Zurowski, M. Labanowska, Polish J. Chem., 69 (1995) 998.
71. H. C. Melville, S. Ekkehard, Inorg. Nucl. Chem, Letters, 5 (1969) 125.
72. V. Gomathy, K. Das, D. Ghosh, J. Phys. C: Solid State Phys., 8 (1975) 158.
73. B.J. Prince, M.M. Turnbull, R.D. Willett, J. Coord. Chem., 56 (2003) 441.
74. M.M. Turnbull, C.P. Landee, B.M. Wells, Coord. Chem. Rev., 249 (2005) 2567.
75. U.Schubert, C.Maurer, M.Bendova, S.Baumann, C.Artner CSD Communication (2020) 2038325. DOI: 10.5517/ccdc.csd.cc26f1f4
76. I.U. Khan, O. Sahin, O. Buyukgungor, Acta Crstallogr. E., 66 (2010) 492.
77. G. L. Miessler, D. A. Tarr, *Inorganic Chemistry*, Pearson Education, 2004, Appx. B.
78. C.P. Landee, M.M. Turnbull, J. Coord. Chem., 67 (2014) 375.
79. O. Kahn, *Molecular Magnetism*, VCH Publishers, New York, 1993, Chap. 3.